Sensors & Transducers, Vol. 229, Issue 1, January 2019, pp. 78-83

www.sensorsportal.com

Sensors & Transducers

Published by IFSA Publishing, S. L., 2019
http://www.sensorsportal.com

Time Encoded Imaging of Neutrons and Photons Using CLYC Detector Equipped with a Dual Mode Collimator

Alexander BARZILOV and Amber GUCKES
University of Nevada Las Vegas, 4505 S. Maryland Parkway, Las Vegas, NV 89154, United States
Tel.: +17028954325, fax: +17028953936
E-mail: alexander.barzilov@unlv.edu

Received: 30 November 2018 /Accepted: 31 December 2018 /Published: 31 January 2019

Abstract: Information about a radiation source's position is essential for methods of simultaneous detection of neutrons and photons. The detection system that is capable of spatial mapping of radiation in two dimensions was developed. A single $Cs_2LiYCl_6:Ce^{3+}$ detector enriched in ^7Li isotope (C^7LYC) was equipped with a hybrid dual-mode rotational collimator. The collimator was designed as a coded aperture (a modified uniformly redundant array) using lead and plastic components. C^7LYC scintillator enables segregation of neutron signals from photon signals, and neutron and photon energy measurements. Radiation measurements were performed at different angular positions of the collimator using a single detector. Maximum likelihood expectation technique was utilized to generate the image of an assayed radiation source. Time encoded imaging of neutron and photon sources was demonstrated using this detection system.

Keywords: C^7LYC, Pulse shape discrimination, Gamma spectroscopy, Neutron detection, Dual mode hybrid collimator, Time encoded imaging.

1. Introduction

Simultaneous measurement of photons and neutrons is used in various detection technologies. Localization of a source position is essential for radiation imaging applications, monitoring of radiation facilities, and for environmental assay of contaminated areas [1-3]. Detector arrays including coded aperture systems and Compton imagers were employed for these directional detection tasks [4-6]. Compton photon imagers and neutron scatter cameras are based on many collisions in order to reconstruct a trajectory of an incident photon or neutron.

These techniques necessitate the use of position-sensitive detectors of high spatial resolution arranged in multiple planes. The encoding of radiation flux in space using a fixed mask and a position-sensitive detector array with small pixels requires numerous signal readout channels. Typically, pixilated arrays have a low detection efficiency, complicated design, and high cost. The use of a rotational coded-aperture collimator allows time encoded imaging based on a single detector with measurements carried out at different angular positions of the collimator.

In this case, the radiation-attenuating mask is not fixed but rotates at a certain angular speed, encoding the radiation flux in time. The measured time (or angle) dependent radiation data enable reconstructing the direction to a source that does not change its position during the assay. It allows using a single detector of large volume to increase the detection efficiency, simplifying the measurement setup and potentially reducing cost of the system. This approach was investigated for the time encoded neutron detection [7-8]. The capability to measure neutrons and photons at the same time requires dual-mode

detectors and hybrid collimators that combine low-Z and high-Z masks to attenuate both radiations. To enable simultaneous imaging of neutron and photon sources in two dimensions, a detection system based on a single C^7LYC scintillator [9] enriched in ^7Li isotope was developed. The system is equipped with a hybrid dual-mode rotational collimator.

2. Experimental System

2.1. Dual Mode Radiation Detector

A 5 cm by 5 cm cylindrical $Cs_2LiYCl_6:Ce^{3+}$ (CLYC) scintillation detector - was used in the experimental system. CLYC's scintillation yields are the following: 2×10^4 photons per 1-MeV gamma ray and 7×10^4 photons per neutron. This scintillation process has three decay components [10]: (a) core-to-valence luminescence (CVL) with 250 nm - 350 nm wavelength range and 2 ns decay time constant; (b) Ce^{3+} prompt emission (350 nm - 450 nm; 50-ns decay constant); (c) cerium self-trapped excitation (Ce-STE) with 1000-ns decay constant.

The scintillation process components (a) and (b) are induced by photon interactions. The (c) component is caused by neutron interactions. Such differences in the decay time enable neutron-photon pulse shape discrimination (PSD) [11]. CLYC has exceptional neutron-photon discrimination properties: the PSD figure of merit [12] is more than 2. As other elpasolite scintillator compounds, this scintillator is capable of a gamma-ray spectroscopy [13]. The CLYC photon energy resolution is ~4 % at 662 keV.

Depending on the lithium content of the CLYC crystal, it can be deployed as a thermal neutron sensor by means of $^6Li(n,\alpha)t$ reaction or as a fast neutron spectrometer by the use of $^{35}Cl(n,p)^{35}S$ reaction (Q = 0.615 MeV). In the latter reaction, the emitted proton's energy is 0.615 MeV plus the incident neutron's energy, so the neutron energy can be deduced from the observed full-energy peak caused by the proton. By increasing the ^7Li fraction and reducing the ^6Li content of CLYC, its fast neutron spectroscopy capability can be optimized by suppressing the thermal-neutron's signature at the 3.2-MeV gamma equivalent energy (GEE) region [14]. Thus, CLYC scintillator enriched with ^7Li is a dual-mode detector that allows neutron and photon energy measurements simultaneously [15].

The 99 % ^7Li enriched C^7LYC detector equipped with a 5-cm diameter super bialkali photomultiplier (PMT) and a voltage generator has a single readout channel. The 12 bit, 80 MSPS eMorpho digitizer was used for processing of the PMT's anode signals. The digitizer connected to a computer via USB cable enabled a list mode - a record for each analyzed waveform contained the event's time stamp, energy, and PSD data. PSD and spectral analysis of list mode data were carried out providing the neutron and photon energy data.

2.2. Multimode Rotational Collimator

The cylindrical dual-mode collimator was assembled as a coded aperture composed of a high density polyethylene (HDPE, a low-Z medium) and lead (Pb, a high-Z medium). A 58×58 elements modified uniformly redundant array (MURA) was employed as the combination of neutron and photon masks inlaid in each other forming a single structure [16]. The MURA array was previously utilized in radiation imaging with a good resolution when used as a flat mask [17]. In the system design, the coded aperture was designed as a curved mask.

To estimate thickness at which neutrons and photons could be attenuated by the HDPE and Pb masks, a parametric study was performed using MCNP6 code [18]. The 7.62 cm thickness was determined optimal for both the HDPE and the Pb. Height of the hybrid collimator is 25.4 cm. The C^7LYC detector was fixed on the frame, on the axis of the collimator. To enable time encoded imaging, the collimator was rotated 360° by a computer-controlled stepper motor. A scheme of the system and experimental setup are shown in Fig. 1(a) and Fig. 1(b).

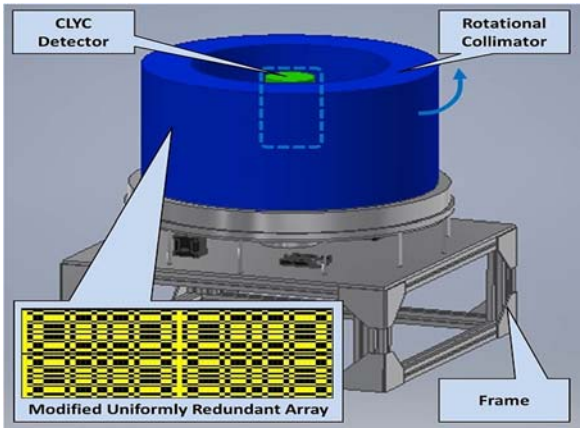

(a)

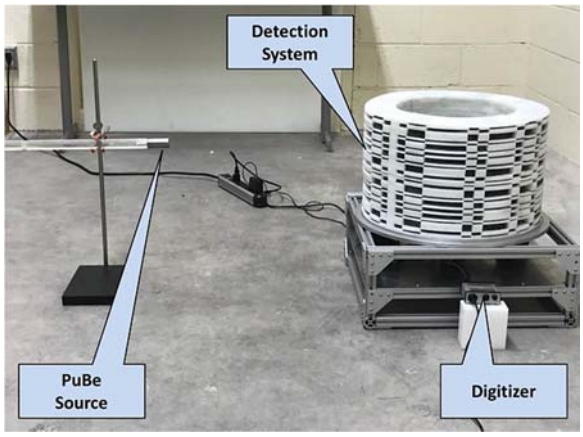

(b)

Fig. 1. (a) Scheme of the detection system; (b) Experimental setup.

2.3. Image Reconstruction

To create an image of a radioactive source, the detector data measured at different angular positions of the hybrid collimator should be convoluted using a decoding mask of the used coded aperture. Maximum likelihood expectation maximization method (MLEM) [19] was utilized for the image reconstruction for both neutron and photon sources. This method was adjusted for the time encoded imaging using the dual-material collimator as follows:

$$\hat{C}_{new}(s_p) = \hat{C}_{old}(s_p) \sum_{t=1}^{T} \frac{N(t) \cdot M(s_p,t)}{\sum_{s_d=1}^{S} \hat{C}_{old}(s_d) \cdot M(s_d,t)}, \quad (1)$$

where s_p is a projected source's pixel in the image, $\hat{C}_{new}(s_p)$ is the count rate estimate at s_p, t is the time, s_d is a dummy variable indicating the projected source's pixel as well, $\hat{C}_{old}(s_p)$ is the previous estimate for the count rate at s_p, $N(t)$ represents counts in the detector at time t, and $M(s,t)$ is the detector's response matrix.

This matrix was formed taking into account attenuation of the incident radiation (photons or neutrons) by the mask (HDPE or Pb) and the position of the collimator at time t:

$$M(s,t) = \frac{I}{I_0} \frac{\cos(\theta(t))}{Z(s)} \left(\frac{1}{1-(D_{col}/D_{det})^2} \right)^{1/2}, \quad (2)$$

where I/I_0 is the fraction of radiation absorbed by the mask, $\theta(t)$ is the angle at time t, $Z(s)$ is the estimated distance between the detector and a possible position of a source, D_{col} is the outer diameter of the collimator, and D_{det} is the detector's diameter. The absorbed radiation fraction in (Eq. (2)) was calculated for photons and neutrons as follows.

For photons:

$$\frac{I}{I_0} = e^{-\left(\frac{\mu}{\rho}\right)\rho X_\gamma}, \quad (3)$$

where μ/ρ is the incident photon energy dependent attenuation coefficient of the absorber, ρ is the absorber's density, and X_γ is the thickness of the photon absorber.

For neutrons:

$$\frac{I}{I_0} = e^{-\sigma A_n X_n}, \quad (4)$$

where σ is the energy-dependent microscopic total neutron cross-section for the absorber, A_n is the absorber's number density, and X_n is the thickness of the absorber.

Attenuation through both Pb and HDPE layers were taken into account in the calculation of the response matrix for the photon (Eq. (3)) and photon cases (Eq. (4)). In the hybrid collimator design, the Pb and HDPE layers had the same thickness.

To process measured radiation data, the MLEM algorithm was implemented using MATLAB. The (Eq. (1)) was iterated until the value of $\hat{C}_{new}(s_p)$ converged to the actual position of a radiation source. Because MLEM assumes a Poisson likelihood of the estimate that converges to the actual source's position, the Poisson noise can induce high-frequency instability which at certain algorithm's iterations generates an incorrect estimate of the location of the source [20]. In order to avoid this instability, the iteration in MLEM algorithms is stopped when the estimate is both converged and agrees with the actual position of the source. This number of iterations is typically found experimentally using known source locations. Using the experimental setup, it was determined that 200 iterations satisfied both conditions; this number of iterations was set in the code as a cutoff parameter.

3. Results and Discussion

To demonstrate photon and neutron time encoded imaging using the dual-mode detector and hybrid collimator, the experimental setup shown in Fig. 1(b) was used [21]. Measurements of gamma and neutron sources were carried out in 58 discrete time steps corresponding to specific angular positions of the hybrid collimator which was rotated 360°.

Two sources - a ^{137}Cs isotope that emits 662 keV gamma rays and ^{60}Co (1173 keV and 1332 keV gamma rays) - were placed at 30° and 60° angular positions, respectively, at a different height above the concrete floor (31 cm and 46 cm) and measured at the same time. Two distances from the collimator surface were used: 29 cm and 100 cm. The results of the reconstruction of positions of these two photon emitters using the MLEM algorithm are shown in Fig. 2(a) and Fig. 2(b). In reconstructed images, *x*- and *y*-coordinates of the source position are shown as a element's numbers of the 58×58 MURA of the collimator. Detector count rates in pixels are indicated using a color scale. Source positions in the 2D image were correctly estimated for both distances from the collimator: the ^{137}Cs source was located at {5; 36} and the ^{60}Co source was at {10; 5}.

A 2-Curie plutonium-beryllium source (PuBe) was used to demonstrate simultaneous imaging of this source using both fast neutrons and photons (Fig. 1(b)). ^{239}Pu isotope is an alpha emitter with a 2.41×10^4 year half-life that produces α-particles with average energy of 5.15 MeV. The α-particles strike beryllium emitting neutrons via (α,*n*) reaction with a specific yield 2.3×10^6 neutrons per second per 1 Curie. Neutron's maximum energy in the PuBe spectrum is 10.7 MeV; mean neutron energy is 4.5 MeV [22]. This source also emits photons causing the γ dose of 6 millirad per hour at 1 m for the yield of 10^6 neutrons per second [23]. Hence, both radiations were measured by C^{7}LYC, then neutron and gamma signals were segregated using PSD.

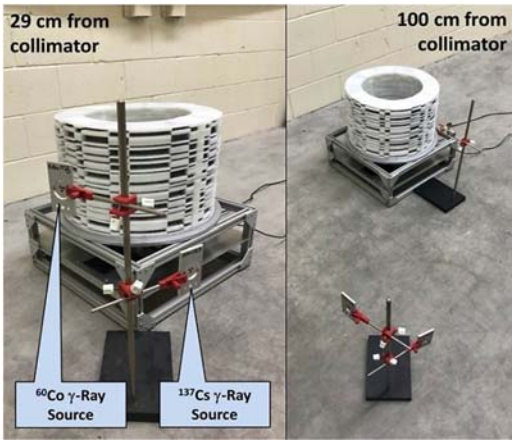

(a)

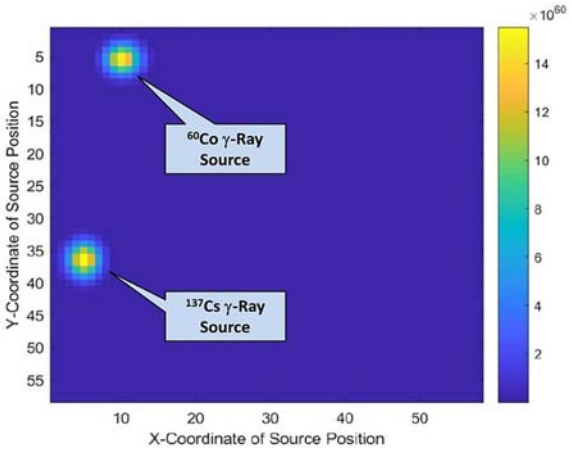

(b)

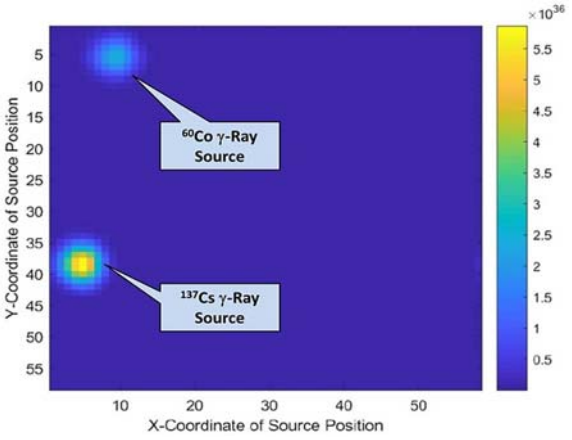

(c)

Fig. 2. (a) Experimental setup; MLEM reconstruction of positions of ^{137}Cs and ^{60}Co photon sources placed at different height in (b) 29 cm and (c) 100 cm from the collimator.

The PuBe source was placed at 50 cm distance from the collimator at 40 cm above the floor at the angular positon 180° which is {30; 17} in the MURA element based coordinates. The estimated source position based on the time encoded imaging of neutrons was {32; 22} as shown in Fig. 3(a). The neutron-based estimate of the PuBe location differs from the actual position by 2 pixels in the *x*-direction and 5 pixels along *y*. The PuBe's position was estimated using the time-encoded photon data as {30; 21} (Fig. 3(b)).

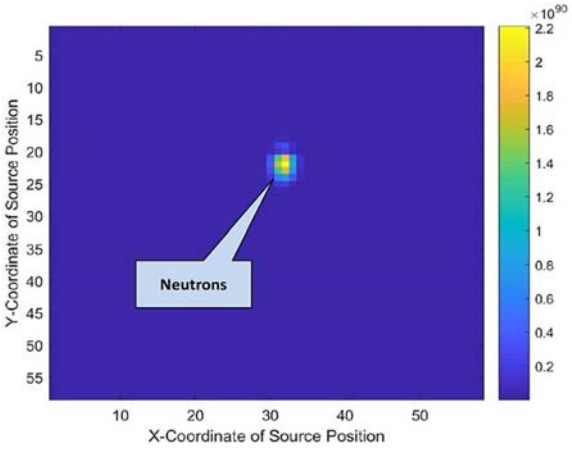

(a)

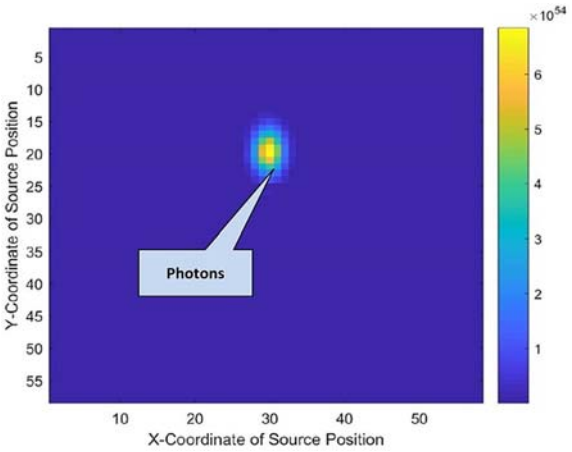

(b)

Fig. 3. Reconstruction of the PuBe source position at {30; 21} using the time encoded (a) neutron data and (b) photon data.

The photon based reconstruction of the (α,*n*) source's position agreed well with neutron based estimates. This is expected because both radiations are emitted by the same source. To verify how the image reconstruction algorithm treats the change of vertical coordinate of the source's position, the PuBe was placed at the same distance from the collimator, but at 30 cm above the floor (10 cm difference from the previous case). This source position had the image coordinates {30; 38}. The MLEM estimated source position using the measured neutron data was {29; 38} (Fig. 4(a)). The difference from the actual position is 1 pixel in *x*-direction. The estimated source position based on the time encoded imaging of photons measured from the same source was {29; 35}. The

discrepancy is 1 pixel in the *x*-direction and 3 pixels in the *y*-direction as shown in Fig. 4(b).

The PuBe source was placed at 1 m away from the collimator's surface at 30 cm above the floor at the angular positon 304°, or {49; 38} in element based coordinates of the 2D image. The MLEM estimated source position using neutrons was {48; 37} as shown in Fig. 5(a). The difference from the actual position of the radiation source is 1 pixel for both *x* and *y* directions. The source's position estimate using photons emitted from the same PuBe source was {51; 42} as shown in Fig. 5(b); the difference from the actual source coordinates is 2 and 4 pixels in the *x* and *y* directions, respectively.

It should be noted that experiments were carried out at the concrete vault that caused neutron scattering from its surfaces. Time encoded measurements of a source that is placed at larger distances from the detection system in the field conditions provide a smaller error in the estimate of the source's position. At larger distance from the collimator, a distributed source appears like a point source. The MURA coded aperture pattern of the hybrid collimator is better suited for point-like sources.

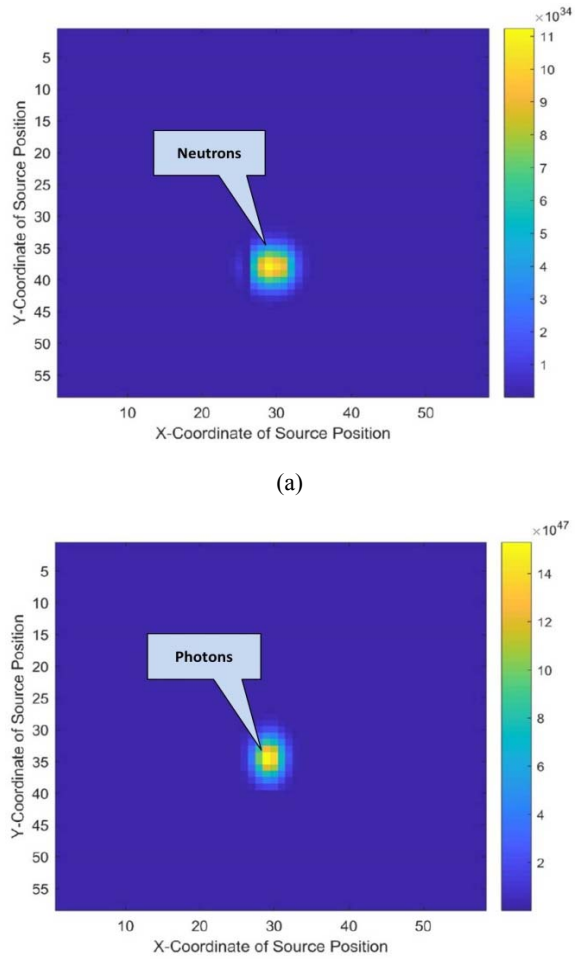

(a) (b)

Fig. 4. Reconstruction of the PuBe source position at [30; 38] elements using the time encoded (a) neutron data and (b) photon data.

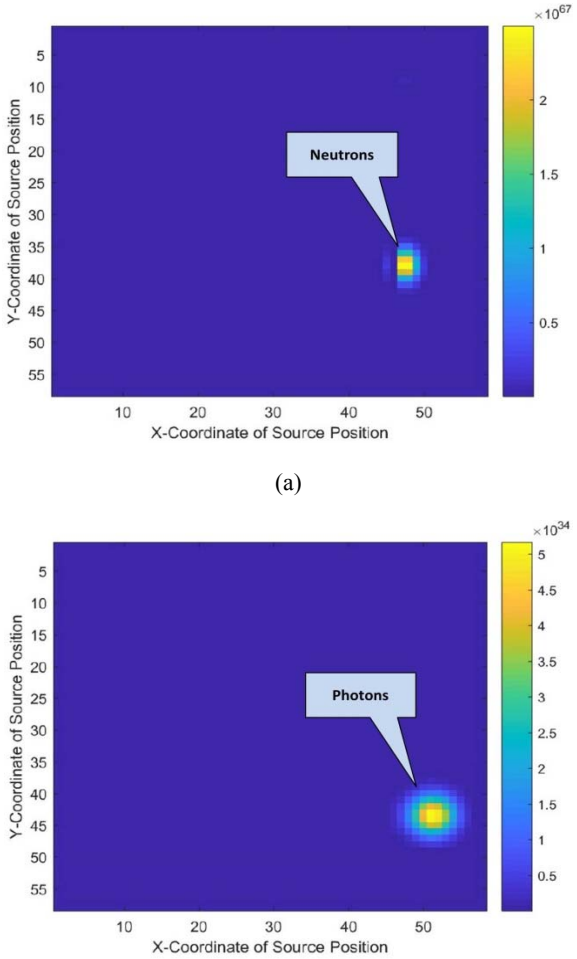

(a) (b)

Fig. 5. MLEM reconstruction of the PuBe source's position placed at 1 m from the collimator's face at the image coordinates {49; 38} using the time encoded (a) neutron data and (b) photon data.

4. Conclusions

The detection system for imaging of neutron and photon sources in two dimensions was developed. It includes a single C^7LYC detector equipped with a rotational collimator - a MURA coded aperture composed of high-Z and low-Z materials (lead and high density polyethylene). The dual-material collimator rotated 360º around the C^7LYC detector enabled the time encoded imaging. The system enables gamma and neutron spectroscopy and effective segregation of neutron and photon signals. The MLEM algorithm developed as a MATLAB code yielded estimates of the source image allowing determining the source's position. Time encoded imaging of neutron and gamma-ray sources was demonstrated using this system.

The time encoded imaging of neutron and photon sources simultaneously proved to be functional using the detection system equipped with the rotational

MURA mask, however, the further improvements are possible. It is envisioned that the next version of the dual mode collimator can be designed using a 3D printed plastic-tungsten compound that contains low- and high-density materials capable of attenuating both neutrons and photons. Moreover, other patterns of the coded aperture mask (i.e., an optimized random pattern, a uniformly redundant array, and others) can be investigated to determine optimal patterns for point source's imaging and imaging of distributed sources.

References

[1]. J. Till, H. Grogan, Radiological risk assessment and environmental analysis, *Oxford University Press*, 2008.

[2]. S. Dewji, D. Lee, S. Croft, N. Hertel, J. Chapman, R. McElroy, S Cleveland, Validation of gamma-ray detection techniques for safeguards monitoring at natural uranium conversion facilities, *Nuclear Instruments and Methods in Physics Research Section A*, Vol. 823, 2016, pp. 135-148.

[3]. K. Moody, I. Hutcheon, P. Grant, Nuclear forensic analysis, *CRC Press*, 2005.

[4]. M. Cieslak, K. Gammage, R. Glover, Coded-aperture imaging systems: past, present and future development - a review, *Radiation Measurements*, Vol. 92, 2016, pp. 59-71.

[5]. R. Woolf, B. Phlips, A. Hutcheson, E. Wulf, Fast-neutron, coded-aperture imager, *Nuclear Instruments and Methods in Physics Research Section A*, Vol. 784, 2015, pp. 398-404.

[6]. T. Lee, W. Lee, Multiple scattering Compton camera with neutron activation for material inspection, *Nuclear Instruments and Methods in Physics Research Section A*, Vol. 784, 2015, pp. 423-429.

[7]. J. Brennan, E. Brubaker, M. Gerling, P. Marleu, K. McMillan, A. Nowack, N. Renard-Le Galloudec, M. Sweany, Demonstration of two-dimensional time-encoded imaging of fast neutrons, *Nuclear Instruments and Methods in Physics Research Section A*, Vol. 802, 2015, pp. 76-81.

[8]. J. Brennan, E. Brubaker, M. Gerling, P. Marleu, M. Monterial, A. Nowack, P. Schuster, B. Sturm, M. Sweany, Source detection at 100 meter standoff with a time-encoded imaging system, *Nuclear Instruments and Methods in Physics Research Section A*, Vol. 877, 2018, pp. 375-383.

[9]. M. Smith, T. Achtzehn, H. Andrews, E. Clifford, P. Forget, J. Glodo, R. Hawrami, H. Ing, P. O'Dougherty, K. Shah, U. Shirwadkar, L. Soundara-Pandian, J. Tower, Fast neutron measurements using Cs_2LiYCl_6:Ce (CLYC) scintillator, *Nuclear Instruments and Methods in Physics Research Section A*, Vol. 784, 2015, pp. 162-167.

[10]. N. D'Olympia, P. Chowdhury, C. J. Lister, J. Glodo, R. Hawrami, K. Shah, U. Shirwadkar, Pulse-shape analysis of CLYC for thermal neutrons, fast neutrons, and gamma-rays, *Nuclear Instruments and Methods in Physics Research Section A*, Vol. 714, 2013, pp. 121-127.

[11]. A. Giaz, L. Pellegri, F. Camera, N. Blasi, S. Brambilla, S. Ceruti, B. Million, S. Riboldi, C. Cazzaniga, G. Gorini, M. Nocente, A. Pietropaolo, M. Pillon, M. Rebai, M. Tardocchi, The CLYC-6 and CLYC-7 response to γ-rays, fast and thermal neutrons, *Nuclear Instruments and Methods in Physics Research Section A*, Vol. 810, 2016, pp. 132-139.

[12]. J. Hartman, A. Barzilov, E. Peters, S. Yates, Measurements of response functions of EJ-299-33A plastic scintillator for fast neutrons, *Nuclear Instruments and Methods in Physics Research Section A*, Vol. 804, 2015, pp. 137-143.

[13]. P. Guss, T. Stampahar, S. Mukhopadhyay, A. Barzilov, A. Guckes, Scintillation properties of a $Cs_2LiLa(Br_6)90\%(Cl_6)10\%:Ce^{3+}$ (CLLBC) crystal, in *Proceedings of the SPIE Radiation Detectors - Systems and Applications Conference XV*, San Diego, USA, 19 - 21 August 2014, Vol. 9215, pp. 921505-1 - 921505-15.

[14]. J. Glodo, W. Higgins, E. van Loef, K. Shah, Cs_2LiYCl_6:Ce scintillator for nuclear monitoring applications, *IEEE Transactions on Nuclear Science*, Vol. 56, Issue 3, 2009, pp. 1257-1261.

[15]. A. N. D'Olympia, P. Chowdhury, C. Guess, T. Harrington, E. Jackson, S. Lakshmi, C. Lister, J. Glodo, R. Hawrami, K. Shah, U. Shirwadkar, Optimizing Cs_2LiYCl_6 for fast neutron spectroscopy, *Nuclear Instruments and Methods in Physics Research Section A*, Vol. 694, 2012, pp. 140-146.

[16]. A. Guckes, A. Barzilov, Development and deployment of the collimated directional radiation detection system, in *Proceedings of the SPIE Conference on Radiation Detectors in Medicine, Industry, and National Security*, San Diego, USA, Vol. 10393, 6 - 10 August 2017, pp. 1039306-1-1039306-10.

[17]. S. Gottesman, E. Fenimore, New family of binary arrays for coded aperture imaging, *Applied Optics*, Vol. 28, Issue 20, 1989, pp. 4344-4352.

[18]. T. Goorley, Initial MCNP6 release overview, *Nuclear Technology*, Vol. 180, Issue 3, 2012, pp. 298-315.

[19]. L. Shepp, Y. Vardi, Maximum likelihood reconstruction for emission tomography, *IEEE Transactions on Medical Imaging*, Vol. MI-1, Issue 2, 1982, pp. 113-122.

[20]. J. De Lima, Nuclear medicine physics, *CRC Press*, 2011.

[21]. A. Barzilov, A. Guckes, Demonstration of simultaneous imaging of neutrons and gamma rays using a CLYC detector with a dual mode rotational collimator, in *Proceedings of Conference on Sensors and Electronic Instrumentation Advances* (*SEIA'18*), Amsterdam, The Netherlands, 19 - 21 September 2018, pp. 110-112.

[22]. R. Evans, The atomic nucleus, *McGraw-Hill Book Company*, 1955.

[23]. Neutron Sources, JPRS-48421, *Joint Publication Research Center*, Washington, DC, 1969.